Weierstraß-Institut

für Angewandte Analysis und Stochastik

Leibniz-Institut im Forschungsverbund Berlin e. V.

Preprint ISSN 0946 – 8633

Geometric error of finite volume schemes for conservation laws on evolving surfaces

Jan Giesselmann[1], Thomas Müller [2]

submitted: January 10, 2013

[1] Weierstrass Institute
Mohrenstr. 39
10117 Berlin
Germany
E-Mail: Jan.Giesselmann@wias-berlin.de

[2] Universität Freiburg
Abteilung für Angewandte Mathematik
Hermann-Herder-Str. 10
79104 Freiburg
Germany
E-mail: mueller@mathematik.uni-freiburg.de

No. 1760

Berlin 2013

2010 *Mathematics Subject Classification.* 65M08, 35L65, 58J45.

Key words and phrases. hyperbolic conservation laws, finite volume schemes, curved surfaces, error bound.

We gratefully acknowledge that the work of T.M. was supported by the German Research Foundation (DFG) via SFB TR 71 'Geometric Partial Differential Equations'. J.G. would like to thank the German Research Foundation (DFG) for financial support of the project 'Modeling and sharp interface limits of local and non-local generalized Navier–Stokes–Korteweg Systems'.

Edited by
Weierstraß-Institut für Angewandte Analysis und Stochastik (WIAS)
Leibniz-Institut im Forschungsverbund Berlin e. V.
Mohrenstraße 39
10117 Berlin
Germany

Fax: +49 30 20372-303
E-Mail: preprint@wias-berlin.de
World Wide Web: http://www.wias-berlin.de/

This paper studies finite volume schemes for scalar hyperbolic conservation laws on evolving hypersurfaces of $\mathbb{R}^3$. We compare theoretical schemes assuming knowledge of all geometric quantities to (practical) schemes defined on moving polyhedra approximating the surface. For the former schemes error estimates have already been proven, but the implementation of such schemes is not feasible for complex geometries. The latter schemes, in contrast, only require (easily) computable geometric quantities and are thus more useful for actual computations. We prove that the difference between approximate solutions defined by the respective families of schemes is of the order of the mesh width. In particular, the practical scheme converges to the entropy solution with the same rate as the theoretical one. Numerical experiments show that the proven order of convergence is optimal.

1 Introduction

Hyperbolic conservation laws serve as models for a wide variety of applications in continuum dynamics. In many applications the physical domains of these problems are stationary or moving hypersurfaces. Examples of the former are in particular geophysical problems [27] and magnetohydrodynamics in the tachocline of the sun [15, 24]. Examples of the latter include transport processes on cell surfaces [22], surfactant flow on interfaces in multiphase flow [5] and petrol flow on a time dependent water surface. There are several recent approaches to the numerical computation of such equations. Numerical schemes for the shallow water equations on a rotating sphere can be found in [6, 16, 23]. For the simulation of surfactant flow on interfaces we refer to [1, 4, 17]. As we are interested in numerical analysis we focus on nonlinear scalar conservation laws as a model for these systems. The intense study of conservation laws posed on fixed Riemannian manifolds started within the last years. There are results about well-posedness [3, 10, 20] of the differential equations and about the convergence of appropriate finite volume schemes [2, 13, 14, 19]. For recent developments on finite volume schemes for parabolic equations we refer to [21].

In the previous error analysis for finite volume schemes approximating nonlinear conservation laws on manifolds the schemes were defined on curved elements lying on the curved surface and it was assumed that geometric quantities like lengths, areas and conormals are known exactly. While this is a reasonable assumption for schemes defined on general Riemannian manifolds or even more general structures [18] with no ambient space, most engineering applications involve equations on hypersurfaces of $\mathbb{R}^3$ and one aims at computing the geometry with the least effort. This is in particular important for moving surfaces where the geometric quantities have to be computed in each time step. Now the question arises to which extent an approximation of the geometry influences the order of convergence of the scheme.

We consider the following initial value problem, posed on a family of closed, smooth hypersurfaces $\Gamma = \Gamma(t) \subset \mathbb{R}^3$. For a derivation cf. [11, 25]. For some $T > 0$, find $u : G_T := \bigcup_{t\in[0,T]} \Gamma(t) \times \{t\} \to \mathbb{R}$ with

$$\dot{u} + u\nabla_\Gamma \cdot v + \nabla_\Gamma \cdot \mathbf{f}(u, \cdot, \cdot) = 0 \qquad \text{in } G_T, \tag{1.1}$$

$$u(\cdot, 0) = u_0 \qquad \text{on } \Gamma(0), \tag{1.2}$$

where v is the velocity of the material points of the surface and $u_0 : \Gamma(0) \to \mathbb{R}$ are initial data. For every $\bar{u} \in \mathbb{R},\ t \in [0, T]$ the flux $\mathbf{f}(\bar{u}, \cdot, t)$ is a smooth vector field tangential to $\Gamma(t)$, which depends Lipschitz on $\bar{u}$ and smoothly on t. Moreover, we impose the following growth condition

$$|\nabla_\Gamma \cdot f(\bar{u}, x, t)| \leq c + c|\bar{u}| \quad \forall\, \bar{u} \in \mathbb{R}, (x, t) \in G_T \tag{1.3}$$

for some constant $c > 0$. By $\dot{u}$ we denote the material derivative of u which is given by

$$\dot{u}(\Phi_t(x), t) := \frac{d}{dt} u(\Phi_t(x), t),$$

where $\Phi_t : \Gamma(0) \to \Gamma(t)$ is a family of diffeomorphisms depending smoothly on t, such that Φ_0 is the identity on $\Gamma(0)$. Obviously this excludes changes of the topology of Γ. We will assume that the movement of the surface and also the family Φ_t is prescribed. A main result of this paper is a bound for the difference between two approximations of u. In particular, we will give an estimate for the difference between the flat approximate and the curved approximate solution. By curved approximate solution we refer to a numerical solution given by a finite volume scheme defined on the curved surface, cf. Section 2.2, and by flat approximate solution we refer to a numerical solution given by a finite volume scheme defined on a polyhedron approximating the surface, cf. Section 2.3. We will see that the arising geometry errors can be neglected compared to the error between the curved approximate solution and the exact solution, i.e. both approximate solutions converge to the entropy solution with the same convergence rate. We will present numerical examples showing that the proven convergence rate is optimal under the assumptions for the numerical analysis. However, for most numerical experiments we observe higher orders of convergence.

Our analysis also indicates that the geometry error poses an obstacle to the construction of higher order schemes. To this end we perform numerical experiments underlining in which manner the order of convergence of the higher order scheme is restricted by the approximation of the geometry. This shows that to obtain higher order convergence also the geometry of the manifold has to be approximated more accurately, cf. [9] in a finite element context.

The outline of this paper is as follows. In Section 2 we review the definition of finite volume schemes on moving curved surfaces and define finite volume schemes on moving polyhedra approximating the surfaces. The approximation errors for geometric quantities are established in Section 3. Section 4 is devoted to estimating the difference between the curved and the flat approximate solution. Finally, numerical experiments are given in Section 5.

2 The Finite Volume Schemes

This section is devoted to the construction of a family of triangulations $\mathcal{T}_h(t)$ of the surfaces suitably linked to polyhedral approximations $\Gamma_h(t)$ of the surfaces. Afterwards we will recall the definition of a finite volume scheme on $\mathcal{T}_h(t)$ which was considered in the hitherto error analysis and define a finite volume scheme on $\Gamma_h(t)$ which is an algorithm only relying on easily computable quantities. We mention that our triangulation as well as the definition of the finite volume scheme on Γ_h is in the same spirit as the one Lenz et al. [21] used for the diffusion equation on evolving surfaces.

2.1 Triangulation

We start by mentioning that there are neighbourhoods $\mathcal{N}(t) \subset \mathbb{R}^3$ of $\Gamma(t)$ such that for every $x \in \mathcal{N}(t)$ there is a unique point $a(x,t) \in \Gamma(t)$ such that

$$x = a(x,t) + d(x,t)\nu_{\Gamma(t)}(a(x,t)), \tag{2.1}$$

where $d(\cdot,t)$ denotes the signed distance function to $\Gamma(t)$ and $\nu_{\Gamma(t)}(a(x,t))$ the unit normal vector to $\Gamma(t)$ pointing towards the non-compact component of $\mathbb{R}^3 \setminus \Gamma(t)$. See [12] for example.

Let us choose a polyhedral surface $\Gamma_h(0) \subset \mathcal{N}(0)$ which consists of flat triangles such that the vertices of $\Gamma_h(0)$ lie on $\Gamma(0)$, and h is the length of the longest edge of $\Gamma_h(0)$. In addition we impose that the restriction of $a|_{\Gamma_h(0)} : \Gamma_h(0) \to \Gamma(0)$ is one-to-one. We define $\Gamma_h(t)$ as the polyhedral surface that is constructed by moving the vertices of $\Gamma_h(t)$ via the diffeomorphism Φ_t and connecting them with straight lines such that all triangulations share the same grid topology. A triangulation $\bar{\mathcal{T}}_h(t)$ of $\Gamma_h(t)$ is automatically given by the decomposition into faces. We define the triangulation $\mathcal{T}_h(t)$ on $\Gamma(t)$ as the image of $\bar{\mathcal{T}}_h(t)$ under $a(\cdot,t)|_{\Gamma_h(t)}$. We will denote the curved cells with $K(t)$ and the curved faces with $e(t)$. A flat quantity corresponding to some curved quantity is denoted by the same letter and a bar, e.g. let $e(t) \subset \Gamma(t)$ be a curved face then $\bar{e}(t) = (a(\cdot,t)|_{\Gamma_h(t)})^{-1}(e(t))$. In order to reflect the fact that all triangulations share the same grid topology we introduce the following misuse of notation. We denote by K the family of all curved triangles relating to the same triangle $\bar{K}(0)$ on $\Gamma_h(0)$. We do the same for $e, \bar{K}, \bar{e}$. Analogously by $\mathcal{T}_h$ we denote the family of such families of triangles K.

For later use we state the following Lemma summarizing geometric properties, whose derivation can be found in [12].

Lemma 2.1. *Let $\Gamma_h(t)$ be a polyhedral approximation of $\Gamma(t)$ as described above then there exists $C = C(T)$ such that for all $t \in [0,T]$*

1. $\nu_{\Gamma(t)} = \nabla d(\cdot,t)$,
2. $\|d(\cdot,t)|_{\Gamma_h(t)}\|_{L^\infty(\Gamma_h(t))} \leq Ch^2$.

We will use the following notation. By $h_{K(t)} := \operatorname{diam}(K(t))$ we denote the diameter of each cell, furthermore $h := \max_{t\in[0,T]} \max_{K(t)} h_{K(t)}$ and $|K(t)|$, $|\partial K(t)|$ are the Hausdorff measures of $K(t)$ and the boundary of $K(t)$ respectively. When we write $e(t) \subset \partial K(t)$ we mean $e(t)$ to be a face of $K(t)$.

We need to impose the following assumption uniformly on all triangulations $\bar{\mathcal{T}}_h(t)$. There is a constant number $\alpha > 0$ such that for each flat cell $\bar{K}(t) \in \bar{\mathcal{T}}_h(t)$ we have

$$\begin{aligned} \alpha h_{\bar{K}(t)}^2 &\leq \left|\bar{K}(t)\right|, \\ \alpha \left|\partial \bar{K}(t)\right| &\leq h_{\bar{K}(t)}. \end{aligned} \tag{2.2}$$

Later on, we will see that (2.2) implies the respective estimate for the curved triangulation, cf. Remark 3.4. A consequence of (2.2) is that $2\alpha^2 h_{\bar{K}(t)}$ is a lower bound of the radius of the inner circle of $\bar{K}(t)$, which implies that the sizes of the angles in $\bar{K}(t)$ are bounded from below. Furthermore we denote by $\kappa(x,t)$ the supremum of the spectral norm of $\nabla \nu_{\Gamma(t)}(x)$. By straightforward continuity and compactness arguments κ is uniformly bounded in space and time.

2.2 The Finite Volume Scheme on Curved Elements

In this section we will briefly review the notion of finite volume schemes on moving curved surfaces. We consider a sequence of times $0 = t_0 < t_1 < t_2 < \dots$ and set $I_n := [t_n, t_{n+1}]$. Moreover we assign to each $n \in \mathbb{N}$ and $K \in \mathcal{T}_h$ the term u_K^n approximating the mean value of u on $\bigcup_{t\in I_n} K(t) \times \{t\}$ and to each $K \in \mathcal{T}_h$ and face $e \subset \partial K$ a numerical flux function $f_{K,e}^n : \mathbb{R}^2 \to \mathbb{R}$, which should approximate

$$⨍_{I_n} ⨍_{e(t)} \langle f(u(x,t),x,t), \mu_{K,e}(x,t)\rangle \, de(t)\, dt, \tag{2.3}$$

where $de(t)$ is the line element, $\mu_{K,e}(x,t)$ is the unit conormal to $e(t)$ pointing outwards from $K(t)$ and $\langle\cdot,\cdot\rangle$ is the standard Euclidean inner product. Please note that $\mu_{K,e}(t)$ is tangential to $\Gamma(t)$. Then the finite volume scheme is given by

$$\begin{aligned} u_K^0 &:= ⨍_{K(0)} u_0(x) d\Gamma(0), \\ u_K^{n+1} &:= \frac{|K(t_n)|}{|K(t_{n+1})|} u_K^n - \frac{|I_n|}{|K(t_{n+1})|} \sum_{e\subset\partial K} |e(t_n)| f_{K,e}^n(u_K^n, u_{K_e}^n), \\ u^h(x,t) &:= u_K^n \quad \text{for } t \in [t_n, t_{n+1}), x \in K(t), \end{aligned} \tag{2.4}$$

where K_e denotes the cell sharing face e with K and $d\Gamma(0)$ is the surface element. For the convergence analysis it was usually assumed [13, 19] that the used numerical fluxes are uniformly Lipschitz, consistent, conservative and monotone. Additionally, the CFL condition

$$t_{n+1} - t_n \leq \frac{\alpha^2 h}{8L} \tag{2.5}$$

has to be imposed to ensure stability, where L is the Lipschitz constant of the numerical fluxes. Lax-Friedrichs fluxes satisfying this condition are usually defined by

$$f_{K,e}^n(u,v) \;:=\; ⨍_{I_n} \frac{1}{2} ⨍_{e(t)} \langle f(u,\cdot,t) \,+\, f(v,\cdot,t), \mu_{K,e}(t)\rangle \, de(t)\, dt \,+\, \lambda(u \,-\, v), \tag{2.6}$$

where $\lambda = \frac{1}{2}\|\partial_u f\|_\infty$ is an artificial viscosity coefficient ensuring the monotonicity of $f_{K,e}^n$ and stabilizing the scheme.

2.3 The Finite Volume Scheme on Flat Elements

In this section we define a finite volume scheme on $\bar{\mathcal{T}}_h$ which is in the same spirit as (2.4) but only relies on easily accessible geometrical information. We assume that f is smoothly extended from G_T to the whole of $\bigcup_{t\in[0,T]} \mathcal{N}(t)\times\{t\}$. We want to point out that the calculation of areas and lengths is straightforward for flat elements. As well, the approximation of integrals can be achieved using quadrature formulas by mapping cells and edges to a standard triangle and the unit interval, respectively, using affine linear maps. In this fashion we obtain for every time $t \in [0,T]$ quadrature operators $Q_{\bar{K}(t)} : C^0(\bar{K}(t)) \to \mathbb{R}$, and $Q_{\bar{e}(t)} : C^0(\bar{e}(t)) \to \mathbb{R}$ of order $p_1, p_2 \in \mathbb{N}$, respectively. In addition for any compact interval $I \subset [0,T]$ the term $Q_I : C^0(\bar{I}) \to \mathbb{R}$ denotes a quadrature operator of order $p_3 \in \mathbb{N}$.

Before we can use the quadrature operators to define numerical fluxes we need to determine the "discrete" conormals. To each flat triangle $\bar{K}(t)$ we fix a unit normal $\bar{\nu}_{\bar{K}(t)}$ by imposing

$$\langle \bar{\nu}_{\bar{K}(t)}, \nu_{\Gamma(t)}(y)\rangle > 0, \tag{2.7}$$

where y is the barycentre of $K(t)$. We will see in Lemma 3.2 that $\bar{\nu}_{\bar{K}(t)}$ converges to $\nu_{\Gamma(t)}(y)$ for $h \to 0$. To each face $\bar{e}(t)$ and adjacent cell $\bar{K}(t)$ there is a unique unit tangent vector $\bar{\mathbf{t}}_{\bar{K}(t),\bar{e}(t)}$ such that $\bar{\nu}_{\bar{K}(t)} \times \bar{\mathbf{t}}_{\bar{K}(t),\bar{e}(t)}$ is a conormal to $\bar{e}(t)$ pointing outward from $\bar{K}(t)$. Hence this vector product is one candidate for $\bar{\mu}_{\bar{K}(t),\bar{e}(t)}$. However in general

$$\bar{\nu}_{\bar{K}(t)} \times \bar{\mathbf{t}}_{\bar{K}(t),\bar{e}(t)} \neq \pm(\bar{\nu}_{\bar{K}_{\bar{e}}(t)} \times \bar{\mathbf{t}}_{\bar{K}_{\bar{e}}(t),\bar{e}(t)}) \tag{2.8}$$

such that a choice like

$$\bar{\mu}_{\bar{K}(t),\bar{e}(t)} = \bar{\nu}_{\bar{K}(t)} \times \bar{\mathbf{t}}_{\bar{K}(t),\bar{e}(t)}$$

would lead to a loss of conservativity of the resulting numerical fluxes. Therefore we choose

$$\bar{\mu}_{\bar{K}(t),\bar{e}(t)} := \frac{1}{2}\left(\bar{\nu}_{\bar{K}(t)} \times \bar{\mathbf{t}}_{\bar{K}(t),\bar{e}(t)} + \bar{\nu}_{\bar{K}_{\bar{e}}(t)} \times \bar{\mathbf{t}}_{\bar{K}(t),\bar{e}(t)}\right).$$

We define a numerical Lax-Friedrichs flux and a finite-volume scheme:

$$\begin{aligned}
\bar{f}_{\bar{K},\bar{e}}(u,v) &:= \frac{1}{|I_n|} Q_{I_n}\left[\frac{1}{2\,|\bar{e}(\cdot)|} Q_{\bar{e}(\cdot)}\left(\langle f(u,\cdot,\cdot) + f(v,\cdot,\cdot), \bar{\mu}_{\bar{K}(\cdot),\bar{e}(\cdot)}\rangle\right)\right] \\
&\qquad + \lambda(u-v), \\
\bar{u}^0_{\bar{K}} &:= \frac{1}{|\bar{K}(0)|} Q_{\bar{K}(0)}(u_0), \\
\bar{u}^{n+1}_{\bar{K}} &:= \frac{|\bar{K}(t_n)|}{|\bar{K}(t_{n+1})|}\bar{u}^n_{\bar{K}} - \frac{|I_n|}{|\bar{K}(t_{n+1})|}\sum_{\bar{e}\subset\partial\bar{K}} |\bar{e}(t_n)|\bar{f}^n_{\bar{K},\bar{e}}(\bar{u}^n_{\bar{K}}, \bar{u}^n_{\bar{K}_{\bar{e}}}), \\
\bar{u}^h(x,t) &:= \bar{u}^n_{\bar{K}}, \quad \text{for } t \in [t_n, t_{n+1}),\ x \in K(t),
\end{aligned} \tag{2.9}$$

for some sufficiently large $\lambda \geq 0$. Note that by $(2.9)_4$ the function $\bar{u}^h$ is defined on G_T.

3 Geometrical Estimates

In this section we derive estimates for the approximation errors of the geometric quantities. Throughout this section we suppress the time dependence of all quantities. All the estimates can be derived uniformly in time. To obtain the geometrical estimates, we introduce the following lift operator.

Definition 3.1. Let $\bar{U} \subset \Gamma_h$ and $\bar{g}$ a function on $\bar{U}$ then we define a function $\bar{g}^l$ on $a|_{\Gamma_h}(\bar{U})$ as

$$\bar{g}^l = \bar{g} \circ a|_{\Gamma_h}^{-1}.$$

Similarly we define the inverse of this lift operator by

$$g^{-l} = g \circ a|_{\Gamma_h}$$

for a function g defined on some $U \subset \Gamma$.

We begin our investigation with the differences between the normal vectors of the flat and curved elements.

Lemma 3.2. *There is a constant C such that for all flat cells $\bar{K}$ and every $y \in \bar{K}$ we have*

$$\left\|\nu_\Gamma^{-l}(y) - \bar{\nu}_{\bar{K}}\right\| \leq Ch. \tag{3.1}$$

The constant C depends on derivatives of d, in particular on κ.

Proof. WLOG we can assume that $\bar{K}$ is a subset of $\{(x, y, 0) \in \mathbb{R}^3 \,|\, y < 0\}$ such that $\bar{e} = \{(s, 0, 0) \in \mathbb{R}^3 \,|\, s \in [0, h_{\bar{e}}]\}$ is one of its faces and $(\nu_\Gamma)_3^{-l}(y) > 0$ for some $y \in \bar{K}$. We start by showing that there exists some constant $C > 0$ such that

$$|(\nu_\Gamma)_i| \leq Ch, \quad \text{for } i = 1, 2. \tag{3.2}$$

We recall that $\nu_\Gamma = \nabla d$, where d is the signed distance function to Γ. As the vertices of Γ_h lie on Γ we know that there exists $(x, y, 0) \in \bar{K}$ such that

$$d(0, 0, 0) = 0,\ d(h_{\bar{e}}, 0, 0) = 0,\ d(x, y, 0) = 0.$$

Hence, the directional derivatives of d with respect to $(x, y, 0)$ and $(1, 0, 0)$ need to vanish somewhere in $\bar{K}$. Thus their absolute value is of order $\mathcal{O}(h)$ on $\bar{K}$. Due to the angle condition (2.2) an analogous inequality also holds for the directional derivative of d with respect to $(0, 1, 0)$. As the directional derivative of d with respect to $(1, 0, 0),\ (0, 1, 0)$ coincides with $(\nu_\Gamma)_1,\ (\nu_\Gamma)_2$, respectively, this proves (3.2). This immediately implies $(\nu_\Gamma)_3 = \pm\sqrt{1 - \mathcal{O}(h^2)} = \pm 1 + \mathcal{O}(h^2)$. By assumption $(\nu_\Gamma)_3 = 1 + \mathcal{O}(h^2)$ everywhere and by (2.7) we have $\bar{\nu}_{\bar{K}} = (0, 0, 1)$ which proves (3.1). □

Lemma 3.3. *For the difference between the length of a curved edge e and the corresponding flat edge $\bar{e}$ we have*

$$\left|\frac{|e|}{|\bar{e}|} - 1\right| \leq Ch^2, \tag{3.3}$$

and for the difference between the area of a curved cell K and the corresponding flat cell $\bar{K}$ we have

$$\left| \frac{|K|}{|\bar{K}|} - 1 \right| \leq Ch^2, \tag{3.4}$$

where C does not depend on h but on κ.

Furthermore let c_e be the parametrization of e over $\bar{e}$ given by $a|_{\bar{e}}$ then we have

$$|\|c_e'(s)\| - 1| \leq Ch^2. \tag{3.5}$$

Proof. We assume without loss of generality that $\bar{K} \subset \mathbb{R}^2 \times \{0\}$. For small enough h we can parametrize the curved cell K according to (2.1) by a parametrization $c = a|_{\bar{K}} : \bar{K} \to K \subset \mathbb{R}^3$ with

$$c(x_1, x_2) = (x_1, x_2, 0) - d(x_1, x_2, 0)\nu_\Gamma(c(x_1, x_2)),$$

where we suppressed the third coordinate in $\bar{K}$. The ratio of volume elements of K and $\bar{K}$ with respect to the parametrization c is given by

$$\sqrt{|g|} := \sqrt{\det(g)},$$

where the matrix g is defined by

$$g = (g_{ij})_{1 \leq i,j, \leq 2} := (\langle \partial_i c, \partial_j c \rangle)_{1 \leq i,j, \leq 2}.$$

For the parametrization c of K we have

$$\partial_i c = e_i - \langle \nabla d, e_i \rangle \, \nu_\Gamma \circ c - d \; \partial_i c \; \left(\nabla \nu_\Gamma\right)^T \circ c \quad \text{for } i = 1, 2,$$

where e_i denotes the i-th standard unit vector. Due to the bounded curvature of Γ and Lemma 2.1 we can show that

$$\partial_i c = e_i - ((\nu_\Gamma)_i \nu_\Gamma) \circ c + \mathcal{O}(h^2) \quad \text{for } i = 1, 2. \tag{3.6}$$

Applying (3.1) we see that

$$\nu_\Gamma = \pm(0, 0, 1) + \mathcal{O}(h) \text{ and } \langle e_i, \nu_\Gamma \rangle = (\nu_\Gamma)_i = \mathcal{O}(h) \quad \text{for } i = 1, 2.$$

Thus, for the matrix g we have

$$g = \begin{pmatrix} 1 + \mathcal{O}(h^2) & \mathcal{O}(h^2) \\ \mathcal{O}(h^2) & 1 + \mathcal{O}(h^2) \end{pmatrix}$$

which implies for the volume element

$$dK = \sqrt{|g|} d\bar{K} = \sqrt{1 + \mathcal{O}(h^2)} d\bar{K} = d\bar{K} + \mathcal{O}(h^2) d\bar{K}. \tag{3.7}$$

Therefore, we arrive at

$$\left| |K| - \left|\bar{K}\right| \right| = \left| \int_{\bar{K}} \sqrt{|g|} - 1 d\bar{K} \right| \leq C \left|\bar{K}\right| h^2$$

for the error of the cell area which proves (3.4).

To prove (3.3) and (3.5) we consider WLOG an edge $\bar{e} = \{(s,0,0)|0 \leq s \leq h_{\bar{e}}\} \subset \partial\bar{K}$, where $h_{\bar{e}}$ denotes the length of $\bar{e}$. The corresponding curved edge e is parametrized by

$$c_e(s) = c(s,0) = (s,0,0) - d(s,0,0)\nu_\Gamma(c_e(s)). \tag{3.8}$$

Due to the bounded curvature of Γ we get for the derivative

$$c_e'(s) = (1,0,0) - \nu_\Gamma(c_e(s))(\nu_\Gamma)_1(c_e(s)) + \mathcal{O}(h^2). \tag{3.9}$$

Applying (3.1) we get

$$\|c_e'(s)\| = 1 + \mathcal{O}(h^2) \tag{3.10}$$

and therefore

$$||e| - |\bar{e}|| = \left| \int_0^{h_{\bar{e}}} \|c_e'(s)\| - 1 \, ds \right| \leq C \, |\bar{e}| \, h^2.$$

□

Remark 3.4. Let us note that an analogous estimate to (2.2) for curved elements is an easy consequence of (2.2), (3.3), (3.4) and the fact $|h_{\bar{K}} - h_K| \leq Ch^2$, which is a consequence of Lemma 3.3.

Lemma 3.5. *There is a constant C (depending on κ) such that for all flat cells $\bar{K}$, all flat edges $\bar{e} \subset \partial\bar{K}$ and every $x \in \bar{e}$ we have*

$$\left|\langle \bar{\mu}_{\bar{K},\bar{e}}, \mathbf{t}^{-l}(x)\rangle\right| \leq Ch^2, \tag{3.11}$$

$$\left|\langle \bar{\mu}_{\bar{K},\bar{e}}, \nu_\Gamma^{-l}(x)\rangle\right| \leq Ch, \tag{3.12}$$

$$\left|\langle \bar{\mu}_{\bar{K},\bar{e}}, \mu_{K,e}^{-l}(x)\rangle - 1\right| \leq Ch^2, \tag{3.13}$$

where $\mathbf{t}$ *denotes a unit tangent vector to* e*. We want to point out that this estimate is independent of the sign of* $\mathbf{t}$.

Proof. It is sufficient to show versions of (3.11) - (3.13) where $\bar{\mu}_{\bar{K},\bar{e}}$ is substituted by $\bar{\nu}_{\bar{K}} \times \bar{\mathbf{t}}_{\bar{K},\bar{e}}$. Then analogous results for $\bar{\nu}_{\bar{K}_{\bar{e}}} \times \bar{\mathbf{t}}_{\bar{K},\bar{e}}$ are immediate. Indeed, estimates (3.11) - (3.13) follow because $\bar{\mu}_{\bar{K},\bar{e}}$ is the mean of the vectors $\bar{\nu}_{\bar{K}_{\bar{e}}} \times \bar{\mathbf{t}}_{\bar{K},\bar{e}}$ and $\bar{\nu}_{\bar{K}} \times \bar{\mathbf{t}}_{\bar{K},\bar{e}}$. Firstly, we address the proof of (3.11). Let the same assumptions as in the proof of Lemma 3.2 hold and in addition let $\bar{e}$ be given by $\{(x,0,0) \in \mathbb{R}^3 \,|\, x \in [0, h_{\bar{e}}]\}$. We obviously have

$$\bar{\nu}_{\bar{K}} \times \bar{\mathbf{t}}_{\bar{K},\bar{e}} = (0,1,0). \tag{3.14}$$

Note that the assumptions of the proof of Lemma 3.3 are satisfied. Hence we can use (3.9) i.e. the parametrization of e given by c satisfies

$$c'(s) = (1,0,0) - \nu_\Gamma(c(s))(\nu_\Gamma)_1(c(s)) + \mathcal{O}(h^2), \tag{3.15}$$

and coincides with $\mathbf{t}(c(s))$ up to standardization. Hence, in view of (3.5) we obtain

$$\mathbf{t}^{-l}(x) = (1,0,0) - \nu_\Gamma(c(s))(\nu_\Gamma)_1(c(s)) + \mathcal{O}(h^2) \tag{3.16}$$

for some $s \in [0, h_{\bar{e}}]$. Combining (3.14) and (3.16) we find using (3.2)

$$\left|\langle \bar{\nu}_{\bar{K}} \times \bar{\mathbf{t}}_{\bar{K},\bar{e}}, \mathbf{t}^{-l}(x)\rangle\right| = |(\nu_\Gamma)_2(c(s))(\nu_\Gamma)_1(c(s))| + \mathcal{O}(h^2) \leq Ch^2,$$

which is (3.11). Concerning (3.12),

$$\left|\langle \bar{\nu}_{\bar{K}} \times \bar{\mathbf{t}}_{\bar{K},\bar{e}}, \nu_\Gamma^{-l}(x)\rangle\right| \leq \left|(\nu_\Gamma^{-l})_2(x)\right| \leq Ch$$

holds because of (3.14) and (3.2). Thus, it remains to show (3.13). By definition $\mathbf{t}^{-l}(x), \nu_\Gamma^{-l}(x), \mu_{K,e}^{-l}(x)$ form an orthonormal basis of $\mathbb{R}^3$ and the vector $\bar{\nu}_{\bar{K}} \times \bar{\mathbf{t}}_{\bar{K},\bar{e}}$ is of unit length. This means that for every $\bar{x}$ in $\bar{e}$ there exist $b_1(\bar{x}), b_2(\bar{x}), b_3(\bar{x}) \in \mathbb{R}$ satisfying $b_1^2(\bar{x}) + b_2^2(\bar{x}) + b_3^2(\bar{x}) = 1$ such that

$$\bar{\nu}_{\bar{K}} \times \bar{\mathbf{t}}_{\bar{K},\bar{e}} = b_1(\bar{x})\mathbf{t}^{-l}(\bar{x}) + b_2(\bar{x})\nu_\Gamma^{-l}(\bar{x}) + b_3(\bar{x})\mu_{K,e}^{-l}(\bar{x}). \tag{3.17}$$

We know from (3.11) and (3.12) that $|b_1(\bar{x})|, |b_2(\bar{x})| \leq Ch$ for some $C > 0$, which implies using Taylor expansion

$$b_3(\bar{x}) = \pm\sqrt{1 + \mathcal{O}(h^2)} = \pm 1 + \mathcal{O}(h^2). \tag{3.18}$$

Note that it only remains to show that in (3.18) the $+$ holds. As b_3 depends continuously on $\bar{x}$ it is sufficient to find one $(\bar{x}_1, 0, 0) \in \bar{K}$ such that $b_3(\bar{x}_1) = 1 + \mathcal{O}(h^2)$. To that end we consider some $\bar{x}_1, \bar{y}_1 > 0$ such that

$$\gamma : (-\bar{y}_1, 0] \longrightarrow \bar{K}, \quad s \mapsto (\bar{x}_1, s, 0)$$

is a curve leaving $\bar{K}$ through $\bar{e}$. By definition the curve $\tilde{\gamma}$ given by

$$\tilde{\gamma}(s) := \gamma(s) - \nu_\Gamma^{-l}(\gamma(s))d(\gamma(s))$$

is a curve in K leaving through e. This means we have

$$0 < \langle \tilde{\gamma}'(0), \mu_{K,e}(\tilde{\gamma}(0))\rangle. \tag{3.19}$$

Due to (3.17), (3.18) and the fact that $\mu_{K,e}$ is of unit length we already know that

$$\mu_{K,e} \equiv \pm(0,1,0) + \mathcal{O}(h). \tag{3.20}$$

We are able to compute

$$\begin{aligned}\tilde{\gamma}'(s) = (0,1,0) - (0,1,0)(\nabla\nu_\Gamma^{-l}(\gamma(s)))^T d(\gamma(s)) - \nu_\Gamma(\tilde{\gamma}(s))\,\langle \nu_\Gamma(\tilde{\gamma}(s)), (0,1,0)\rangle \\ = (0,1,0) + \mathcal{O}(h),\end{aligned} \tag{3.21}$$

because $\nabla\nu_\Gamma^{-l}$ is bounded, Lemma 2.1 and (3.2). Inserting (3.20) and (3.21) in (3.19) we find

$$0 < \pm 1 + \mathcal{O}(h), \tag{3.22}$$

where $\pm$ is the sign from (3.18). Obviously for h sufficiently small (3.22) only holds for "+", which finishes the proof. □

4 Estimating the Difference Between Both Schemes

This section is devoted to establishing a bound for the difference between the curved and flat approximate solutions. To start with we investigate the difference between the numerical fluxes defined on the flat and the curved triangulation respectively.

Lemma 4.1. *Let $\mathcal{K}$ be some compact subset of $\mathbb{R}^2$. Provided the quadrature operators $Q_{\bar{e}(t)}$ and Q_{I_n} are of order at least 1, then there is a constant C depending only on G_T and $\mathcal{K}$ such that for the Lax-Friedrichs fluxes* (2.6) *and* $(2.9)_1$ *with the same diffusion rate λ the following inequality holds*

$$\left| f^n_{K,e}(u,v) - \bar{f}^n_{\bar{K},\bar{e}}(u,v) \right| \leq Ch^2 \qquad \forall\, (u,v) \in \mathcal{K},\ K \in \mathcal{T}_h,\ e \subset \partial K.$$

Proof. We start by observing that the diffusive terms drop out, such that

$$\begin{aligned} 2\left| f^n_{K,e}(u,v) - \bar{f}^n_{\bar{K},\bar{e}}(u,v) \right| = \Bigg| & \fint_{I_n} \fint_{e(t)} \langle f(u,x,t), \mu_{K(t),e(t)}(x)\rangle de(t)\, dt \\ & - \frac{1}{|I_n|} Q_{I_n}\left[\frac{1}{|\bar{e}(\cdot)|} Q_{\bar{e}(\cdot)}[\langle f(u,\cdot,\cdot), \bar{\mu}_{\bar{K}(\cdot),\bar{e}(\cdot)}\rangle] \right] \\ & + \fint_{I_n} \fint_{e(t)} \langle f(v,x,t), \mu_{K(t),e(t)}(x)\rangle de(t)\, dt \\ & - \frac{1}{|I_n|} Q_{I_n}\left[\frac{1}{|\bar{e}(\cdot)|} Q_{\bar{e}(\cdot)}[\langle f(v,\cdot,\cdot), \bar{\mu}_{\bar{K}(\cdot),\bar{e}(\cdot)}\rangle] \right] \Bigg|. \end{aligned} \tag{4.1}$$

As u and v appear symmetrically we will omit all terms containing the latter in our subsequent analysis. We now add zero several times in (4.1) and get

$$2\left| f^n_{K,e}(u,v) - \bar{f}^n_{\bar{K},\bar{e}}(u,v) \right| = \left| \fint_{I_n} T_1 + T_2 + T_3 + T_4 + T_5\, dt \right| \tag{4.2}$$

with

$$\begin{aligned} T_1(t) &:= \fint_{e(t)} \langle f(u,x,t), \mu_{K(t),e(t)}(x)\rangle de(t) - \fint_{\bar{e}(t)} \langle f^{-l}(u,x,t), \mu^{-l}_{K(t),e(t)}(x)\rangle d\bar{e}(t), \\ T_2(t) &:= \fint_{\bar{e}(t)} \langle f^{-l}(u,x,t), \mu^{-l}_{K(t),e(t)}(x)\rangle d\bar{e}(t) - \fint_{\bar{e}(t)} \langle f^{-l}(u,x,t), \bar{\mu}_{\bar{K}(t),\bar{e}(t)}\rangle d\bar{e}(t) \\ T_3(t) &:= \fint_{\bar{e}(t)} \langle f^{-l}(u,x,t), \bar{\mu}_{\bar{K}(t),\bar{e}(t)}\rangle d\bar{e}(t) - \fint_{\bar{e}(t)} \langle f(u,x,t), \bar{\mu}_{\bar{K}(t),\bar{e}(t)}\rangle d\bar{e}(t) \\ T_4(t) &:= \fint_{\bar{e}(t)} \langle f(u,x,t), \bar{\mu}_{\bar{K}(t),\bar{e}(t)}\rangle d\bar{e}(t) - \frac{1}{|I_n|} Q_{I_n}\left[\fint_{\bar{e}(\cdot)} \langle f(u,x,\cdot), \bar{\mu}_{\bar{K}(\cdot),\bar{e}(\cdot)}\rangle d\bar{e}(\cdot) \right] \\ T_5 &:= \frac{1}{|I_n|} Q_{I_n}\left[\fint_{\bar{e}(\cdot)} \langle f(u,x,\cdot), \bar{\mu}_{\bar{K}(\cdot),\bar{e}(\cdot)}\rangle d\bar{e}(\cdot) - \frac{1}{|\bar{e}(\cdot)|} Q_{\bar{e}(\cdot)}\left[\langle f(u,\cdot,\cdot), \bar{\mu}_{\bar{K}(\cdot),\bar{e}(\cdot)}\rangle \right] \right]. \end{aligned}$$

In the following we will estimate the summands one by one. First, by properties of the quadrature operators Q_{I_n}, $Q_{\bar{e}(t)}$ and the CFL condition (2.5)

$$\left| \fint_{I_n} T_4(t)\, dt \right| \leq Ch^{p_3+1}, \qquad |T_5| \leq Ch^{p_2+1}, \tag{4.3}$$

as the integrands are sufficiently smooth. In particular, we use the fact that the surface evolves smoothly. Addressing the estimates for T_1, T_2, T_3 we will omit the time dependency as all three estimates are uniform in time. To establish an estimate for T_1 we recall that we can parametrize e over $\bar{e}$ such that for the parametrisation c_e inequality (3.5) holds. We have

$$|T_1| = \left| \fint_{\bar{e}} \langle f^{-l}(u,x), \mu_{K,e}^{-l}(x) \rangle \left(\|c_e'(s)\| - 1 \right) d\bar{e} \right| \leq \|f\|_\infty C h^2, \tag{4.4}$$

where $\|f\|_\infty$ denotes the supremum of $f(u,x,t)$ for $(x,t) \in G_T$ and $u \in \mathcal{K}$. Next we turn to T_3. Its estimate is based on the assumption that we have extended $f(u,\cdot)$ to $\mathcal{N}$ smoothly and on the second statement of Lemma 2.1. This leads to

$$|T_3| \leq \fint_{\bar{e}} \left\| f^{-l}(u,x) - f(u,x) \right\| \left\| \bar{\mu}_{\bar{K},\bar{e}} \right\| \, d\bar{e} \leq C h^2. \tag{4.5}$$

This leaves T_2. It is clear that

$$|T_2| \leq \max_{x \in \bar{e}} \left| \langle f^{-l}(u,x), \mu_{K,e}^{-l}(x) - \bar{\mu}_{\bar{K},\bar{e}} \rangle \right|. \tag{4.6}$$

Furthermore we find, as f is tangential to Γ,

$$f^{-l}(u,x) = f_1(u,x) \mathbf{t}^{-l}(x) + f_2(u,x) \mu_{K,e}^{-l}(x),$$

where $\mathbf{t}$ is a unit tangent vector to e and $f_1(u,x), f_2(u,x) \in \mathbb{R}$. Due to Lemma 3.5 we have

$$\langle f^{-l}(u,x), \mu_{K,e}^{-l}(x) \rangle = f_2(u,x), \tag{4.7}$$

$$\langle f^{-l}(u,x), \bar{\mu}_{\bar{K},\bar{e}} \rangle = f_1(u,x) \mathcal{O}(h^2) + f_2(u,x) + f_2(u,x) \mathcal{O}(h^2). \tag{4.8}$$

Obviously it holds $|f_1(u,x)|, |f_2(u,x)| \leq \|f\|_\infty$ such that inserting (4.7),(4.8) into (4.6) gives

$$|T_2| \leq C h^2. \tag{4.9}$$

Now the statement of the Lemma follows from (4.2) together with (4.3), (4.4), (4.5) and (4.9). □

Our next step is to establish stability estimates for the curved and flat approximate solution. Due to the geometry change of the surface Γ which might act as a source term we need the following lemma.

Lemma 4.2. *For every finite sequence of positive numbers $\{b_n\}_{n=1,\dots,N}$ we have*

$$\prod_{n=1}^{N} (1 + b_n) \leq \left(1 + \sum_{n=1}^{N} \frac{b_n}{N} \right)^N \leq \exp\left(\sum_{n=1}^{N} b_n \right). \tag{4.10}$$

Proof. From Jensen's inequality we know

$$\sum_{n=1}^{N} \ln(1 + b_n) \leq N \ln\left(\sum_{n=1}^{N} \frac{1 + b_n}{N} \right). \tag{4.11}$$

Applying the exponential function to (4.11) gives the first inequality in (4.10). The second inequality in (4.10) follows from the fact that

$$\left(1+\frac{c}{N}\right)^N \leq \exp(c) \quad \forall N \in \mathbb{N}, c \in \mathbb{R}.$$

□

Now we can show a stability estimate for the curved scheme, the proof of which is mostly standard.

Lemma 4.3. *Provided the initial data satisfy $u_0 \in L^\infty(\Gamma(0))$, then the solution of the curved scheme fulfils*

$$|u_K^{n+1}| \leq (1+c|I_n|)\max\{|u_K^n|, \max_{e\subset\partial K}\{|u_{K_e}^n|\}\} + c|I_n| \quad \forall\, K \in \mathcal{T}_h, \tag{4.12}$$

for some constant c and therefore

$$\|u^h(t)\|_{L^\infty} \leq (\|u_0\|_{L^\infty} + cT)\exp(cT) \quad \forall\, 0 \leq t \leq T. \tag{4.13}$$

Proof. Invoking the consistency of the numerical flux functions we can rewrite (2.4)

$$u_K^{n+1} = \frac{|K(t_n)|}{|K(t_{n+1})|}\left((1-\sum_{e\subset\partial K} c_{K,e})u_K^n + \sum_{e\subset\partial K} c_{K,e}u_{K_e}^n \right.$$
$$\left. -|I_n| \fint_{I_n}\fint_{K(t_n)} \nabla_\Gamma \cdot f(u_K^n, x, t)\, d\Gamma(t)dt\right)$$

with

$$c_{K,e} = \frac{|I_n|\,|e(t_n)|}{|K(t_n)|}\frac{f_{K,e}^n(u_K^n, u_{K_e}^n) - f_{K,e}^n(u_K^n, u_K^n)}{u_K^n - u_{K,e}^n}.$$

Due to the monotonicity of the numerical fluxes and the CFL condition (2.5) we have

$$c_{K,e} \geq 0, \sum_{e\subset\partial K} c_{K,e} \leq 1.$$

Combining the growth condition (1.3) and the fact that $|K(t_n)|/|K(t_{n+1})| \leq 1 + c|I_n|$ we get (4.12) for a new, possibly larger constant c. Iteration of (4.12) implies

$$\max_{K\in\mathcal{T}_h}|u_K^n| \leq \prod_{k=0}^{n-1}(1+c|I_k|)\max_{K\in\mathcal{T}_h}|u_K^0| + \sum_{k=0}^{n-1} c|I_k| \prod_{j=k+1}^{n-1}(1+c|I_j|). \tag{4.14}$$

Invoking (4.10) we obtain from (4.14)

$$\max_{K\in\mathcal{T}_h}|u_K^n| \leq \exp(cT)\|u_0\|_{L^\infty} + \sum_{k=0}^{n-1} c|I_k|\exp(cT) \leq (\|u_0\|_{L^\infty} + cT)\exp(cT).$$

□

As a technical ingredient for the stability estimate of the flat scheme and the error estimate we need the following lemma whose proof is given in the appendix.

Lemma 4.4. *For times t_n, t_{n+1} and corresponding cells $K(t_n)$, $K(t_{n+1})$, $\bar{K}(t_n)$, $\bar{K}(t_{n+1})$ the following estimates hold*

$$\left| \frac{|K(t_n)|}{|\bar{K}(t_n)|} - \frac{|K(t_{n+1})|}{|\bar{K}(t_{n+1})|} \right| \leq Ch|t_{n+1} - t_n|, \tag{4.15}$$

$$\left| \frac{|\bar{K}(t_n)|}{|\bar{K}(t_{n+1})|} \frac{|K(t_{n+1})|}{|K(t_n)|} - 1 \right| \leq Ch|t_{n+1} - t_n|. \tag{4.16}$$

The stability estimate for the flat scheme is a combination of the stability estimate of the curved scheme and the estimate for the difference of the fluxes.

Lemma 4.5. *Provided the initial data satisfy $u_0 \in L^\infty(\Gamma(0))$, then the solution of the flat scheme fulfils*

$$|\bar{u}_{\bar{K}}^{n+1}| \leq (1 + 2(c+1)|I_n|) \max\{|\bar{u}_{\bar{K}}^n|, \max_{\bar{e} \subset \partial \bar{K}} \{|\bar{u}_{\bar{K}_{\bar{e}}}^n|\}\} + 2(c+1)|I_n| + d|I_n|h \tag{4.17}$$

for all $K \in \mathcal{T}_h$ and $0 \leq t_{n+1} \leq T$. Here c can be chosen as the same constant as in Lemma 4.3 and $d > 0$ is another constant. Therefore, for h sufficiently small,

$$\|\bar{u}^h(t)\|_{L^\infty} \leq (\|u_0\|_{L^\infty} + bT) \exp(bT) + 1, \quad \forall\, 0 \leq t \leq T, \tag{4.18}$$

where $b := 2(c+1)$.

Proof. We have

$$\begin{aligned} \bar{u}_{\bar{K}}^{n+1} =& \frac{|\bar{K}(t_n)|}{|\bar{K}(t_{n+1})|} \left(\bar{u}_K^n - \frac{|I_n|}{|\bar{K}(t_n)|} \sum_{\bar{e} \subset \partial \bar{K}} |\bar{e}(t_n)| \bar{f}_{\bar{K},\bar{e}}^n(\bar{u}_{\bar{K}}^n, \bar{u}_{\bar{K}_{\bar{e}}}^n) \right) \\ =& \frac{|\bar{K}(t_n)|}{|\bar{K}(t_{n+1})|} \left(\bar{u}_{\bar{K}}^n - \frac{|I_n|}{|K(t_n)|} \sum_{e \subset \partial K} |e(t_n)| f_{K,e}^n(\bar{u}_{\bar{K}}^n, \bar{u}_{\bar{K}_{\bar{e}}}^n) \right. \\ & \left. + |I_n| \sum_{e \subset \partial K} \left(\frac{|e(t_n)|}{|K(t_n)|} f_{K,e}^n(\bar{u}_{\bar{K}}^n, \bar{u}_{\bar{K}_{\bar{e}}}^n) - \frac{|\bar{e}(t_n)|}{|\bar{K}(t_n)|} \bar{f}_{\bar{K},\bar{e}}^n(\bar{u}_{\bar{K}}^n, \bar{u}_{\bar{K}_{\bar{e}}}^n) \right) \right). \end{aligned} \tag{4.19}$$

We observe that because of (4.16)

$$\begin{aligned} \frac{|\bar{K}(t_n)|}{|\bar{K}(t_{n+1})|} = \frac{|K(t_n)|}{|K(t_{n+1})|} \frac{|\bar{K}(t_n)|}{|\bar{K}(t_{n+1})|} \frac{|K(t_{n+1})|}{|K(t_n)|} \\ \leq (1 + c\,|I_n|) \cdot (1 + C\,|I_n|\,h) \leq 1 + (c+1)\,|I_n|\,, \end{aligned} \tag{4.20}$$

where c is the same constant as in Lemma 4.3, for h small enough. Moreover, provided $\max_{K \in \mathcal{T}_h} |\bar{u}_{\bar{K}}^n| \leq A + 1 := (\|u_0\|_{L^\infty} + bT) \exp(bT) + 1$ we have

$$\frac{|\bar{K}(t_n)|}{|\bar{K}(t_{n+1})|} \left(\frac{|e(t_n)|}{|K(t_n)|} f_{K,e}^n(\bar{u}_{\bar{K}}^n, \bar{u}_{\bar{K}_{\bar{e}}}^n) - \frac{|\bar{e}(t_n)|}{|\bar{K}(t_n)|} \bar{f}_{\bar{K},\bar{e}}^n(\bar{u}_{\bar{K}}^n, \bar{u}_{\bar{K}_{\bar{e}}}^n) \right) \leq Ch \tag{4.21}$$

because of (3.3), (3.4), and Lemma 4.1. Here we have used that for $|u|, |v| \leq A + 1$, the numerical fluxes $f_{K,e}^n(u, v)$, $\bar{f}_{\bar{K},\bar{e}}^n(u, v)$ are uniformly bounded.

Provided $\max_{K\in\mathcal{T}_h}|\bar{u}^n_{\bar{K}}| \leq A+1$ and $h, |I_n|$ sufficiently small, we obtain (4.17) by the same argumentation as in the proof of Lemma 4.3 for some $d>0$. As obviously $\|\bar{u}^h(0)\|_{L^\infty} \leq A+1$ we have by induction

$$\max_{K\in\mathcal{T}_h}|\bar{u}^n_K| \leq \prod_{k=0}^{n-1}(1+b|I_k|)\max_{K\in\mathcal{T}_h}|\bar{u}^0_K| + \sum_{k=0}^{n-1}(b|I_k|+dh|I_k|)\prod_{j=k+1}^{n-1}(1+b|I_j|)$$
$$\leq \underbrace{(\|u_0\|_{L^\infty}+bT)\exp(bT)}_{\leq A} + dT\exp(bT)h, \quad (4.22)$$

where $b=2(c+1)$. Equation (4.22) shows that our induction hypothesis, $\max_{K\in\mathcal{T}_h}|\bar{u}^n_{\bar{K}}| \leq A+1$, also holds for the next time step provided $h < \frac{1}{\exp(bT)dT}$ and $t_n \leq T$. This implies that (4.17) and (4.22) in fact hold for all $t_n \leq T$. Thus, provided h is small enough, the assertion of the lemma follows by induction. □

In addition we need the fact that the curved scheme satisfies a discrete L^1-contraction property.

Lemma 4.6. *For given data u^n_K and v^n_K, let u^{n+1}_K and v^{n+1}_K, be defined according to the curved finite volume scheme* (2.4)*. Then*

$$\sum_K |K(t_{n+1})||u^{n+1}_K - v^{n+1}_K| \leq \sum_K |K(t_n)||u^n_K - v^n_K|.$$

The proof is analogous to the proof of the discrete L^1-contraction property for finite volume schemes in Euclidean space, cf. [7]. We recall that the Lax-Friedrichs flux (2.6) satisfies the classical conservation and monotonicity conditions.

For the difference between the curved and flat approximate solutions we obtain the following estimate.

Theorem 4.7. *Provided the quadrature operators $Q_{\bar{e}(t)}$ and Q_{I_n} are of order at least 1 for all t, n and the quadrature operators $Q_{K(0)}$ and the initial data u_0 are such that*

$$\|u^h(0) - \bar{u}^h(0)\|_{L^1(\Gamma(0))} \leq C\,h \quad (4.23)$$

for some constant C. Then, for fixed $T>0$, the error between the solution u^h of the curved finite volume scheme (2.4) *and the solution $\bar{u}^h$ of the flat finite volume scheme* (2.9) *satisfies*

$$\left\|u^h(T) - \bar{u}^h(T)\right\|_{L^1(\Gamma(T))} \leq C\,h.$$

for some constant C depending on T, G_T, f, u_0, provided the same diffusion rate λ is used in both schemes.

Remark 4.8. The curved approximate solution converges to the entropy solution of (1.1)-(1.2) with a convergence rate of $\mathcal{O}(h^{1/4})$, cf. [14]. Hence, invoking Theorem 4.7 the same kind of error bound holds for the flat approximate solution.

of Theorem 4.7. Let $n \in \mathbb{N}$ be such that $T \in [t_n, t_{n+1})$, then we have

$$\begin{aligned}
\|u^h(T) - \bar{u}^h(T)\|_{L^1(\Gamma)} &= \sum_K |K(t_{n+1})| \left| u_K^{n+1} - \bar{u}_{\bar{K}}^{n+1} \right| \\
&= \sum_K \Bigg| |K(t_n)| u_K^n - |I_n| \sum_{e \subset \partial K} |e(t_n)| \, f_{K,e}^n(u_K^n, u_{K_e}^n) \\
&\qquad - \frac{|K(t_{n+1})| \, |\bar{K}(t_n)|}{|\bar{K}(t_{n+1})|} \bar{u}_{\bar{K}}^n + |I_n| \frac{|K(t_{n+1})|}{|\bar{K}(t_{n+1})|} \sum_{e \subset \partial K} |\bar{e}(t_n)| \, \bar{f}_{\bar{K},\bar{e}}^n(\bar{u}_{\bar{K}}^n, \bar{u}_{\bar{K}_{\bar{e}}}^n) \Bigg| \\
&\leq R_1 + R_2 + R_3 + R_4 + R_5,
\end{aligned}$$

where

$$\begin{aligned}
R_1 &:= \sum_K \Big| |K(t_n)| u_K^n - |I_n| \sum_{e \subset \partial K} |e(t_n)| \, f_{K,e}^n(u_K^n, u_{K_e}^n) \\
&\qquad - |K(t_n)| \bar{u}_{\bar{K}}^n + |I_n| \sum_{e \subset \partial K} |e(t_n)| \, f_{K,e}^n(\bar{u}_{\bar{K}}^n, \bar{u}_{\bar{K}_{\bar{e}}}^n) \Big| \\
R_2 &:= \sum_K \left| |K(t_n)| \bar{u}_{\bar{K}}^n - \frac{|K(t_{n+1})| \, |\bar{K}(t_n)|}{|\bar{K}(t_{n+1})|} \bar{u}_{\bar{K}}^n \right| \\
R_3 &:= \sum_K |I_n| \sum_{e \subset \partial K} \big| |e(t_n)| - |\bar{e}(t_n)| \big| \left| f_{K,e}^n(\bar{u}_{\bar{K}}^n, \bar{u}_{\bar{K}_{\bar{e}}}^n) \right| \\
R_4 &:= \sum_K \left| \left(1 - \frac{|K(t_{n+1})|}{|\bar{K}(t_{n+1})|} \right) |I_n| \sum_{e \subset \partial K} |\bar{e}(t_n)| \left| f_{K,e}^n(\bar{u}_{\bar{K}}^n, \bar{u}_{\bar{K}_{\bar{e}}}^n) \right| \right| \\
R_5 &:= \sum_K |I_n| \frac{|K(t_{n+1})|}{|\bar{K}(t_{n+1})|} \sum_{e \subset \partial K} |\bar{e}(t_n)| \left| f_{K,e}^n(\bar{u}_{\bar{K}}^n, \bar{u}_{\bar{K}_{\bar{e}}}^n) - \bar{f}_{\bar{K},\bar{e}}^n(\bar{u}_{\bar{K}}^n, \bar{u}_{\bar{K}_{\bar{e}}}^n) \right|.
\end{aligned}$$

Because we consider the Lax-Friedrichs flux which is conservative and monotone and due to the CFL-condition (2.5), term R_1 can be estimated via the discrete L^1-contraction property (Lemma 4.6)

$$R_1 \leq \sum_K |K(t_n)| \, |u_K^n - \bar{u}_{\bar{K}}^n| \, .$$

The term R_2 can be estimated using (4.15), we get

$$R_2 \leq \sum_K |\bar{u}_{\bar{K}}^n| \, |\bar{K}(t_n)| \underbrace{\left| \frac{|K(t_n)|}{|\bar{K}(t_n)|} - \frac{|K(t_{n+1})|}{|\bar{K}(t_{n+1})|} \right|}_{\leq C|I_n|h} \leq C|I_n|h. \tag{4.24}$$

Applying Lemma 3.3 and assumption (2.2) together with Remark 3.4 we get

$$R_3, R_4 \leq \sum_K |I_n| \sum_{e \in \subset \partial K} Ch^3 \left| f_{K,e}^n(\bar{u}_{\bar{K}}^n, \bar{u}_{\bar{K}_{\bar{e}}}^n) \right| \leq C|I_n|h. \tag{4.25}$$

Based on Lemma 3.3, assumption (2.2), Remark 3.4 and Lemma 4.1 we have

$$R_5 \leq C \sum_K |I_n| \sum_{e \subset \partial K} h^3 \leq C|I_n|h. \tag{4.26}$$

Combining these estimates we thus obtain by iteration

$$\begin{aligned}
\left\|u^h(T) - \bar{u}^h(T)\right\|_{L^1(\Gamma)} &= \sum_K |K(t_{n+1})| \left|u_K^{n+1} - \bar{u}_{\bar{K}}^{n+1}\right| \\
&\leq \sum_K |K(t_n)| \left|u_K^n - \bar{u}_{\bar{K}}^n\right| + C|I_n|\, h \\
&\leq \sum_K |K(0)| \left|u_K^0 - \bar{u}_{\bar{K}}^0\right| + CT\, h \\
&\leq C(T+1)h,
\end{aligned}$$

where the last step follows with (4.23). □

5 Numerical Experiments

Numerical investigations based on the finite volume schemes defined in Section 2 are presented in this section. The upshot of our experiments is three-fold. Firstly, under the present assumptions the order of convergence stated in Theorem 4.7 is optimal. This is demonstrated by Test Problem 1. Secondly, all of our experiments which include a sufficiently large numerical viscosity, i.e. $\lambda \in \Theta(1)$ in (2.6), lead to a considerably higher experimental order of convergence (EOC) between 1 and 2 for the L^1-difference between the flat and the curved approximate solution. Thirdly, the application of a finite volume scheme of second order to Test Problem 1 demonstrates that orders of convergence higher than 1 are not to be expected in general, if the geometry is not approximated sufficiently well, see Test Problem 5. In the following we will present several test cases. Thereafter, we will mention some implementation aspects.

5.1 Test Problems

All test cases except Test Problem 7 use the geometrical setting $G_T = \mathbb{S}^2 \times [0,1]$, i.e. $\Gamma(t) = \mathbb{S}^2$ for all $t \in [0,T]$, and $T = 1$. This is due to the fact, that we are able to compute the exact curved quantities only in this or similarly simple settings. In addition, let us fix the vector fields $V(x) = \frac{2\pi}{\|x\|}(x_2, -x_1, 0)^T$ and $W(x) = \frac{2\pi}{\|x\|}(-x_3, 0, x_1)^T$ for $x = (x_1, x_2, x_3) \in \mathbb{S}^2$.

Test Problem 1 (u-independent flux function). We choose $f = V$ as the flux function. Since f neither depends on t nor on u and is divergence-free on $\mathbb{S}^2$ any initial datum $u_0 : \mathbb{S}^2 \to \mathbb{R}$ is a stationary solution of the corresponding initial value problem (1.1)-(1.2). For initial values identically to zero the curved scheme conserves this stationary solution. Thus, the error between the curved and the flat approximate solution is equal to the error between the flat approximate solution and the exact solution. The results for this test case for $\lambda = 0$ are plotted in Table 1. Note that due to $\partial_u f = 0$ the numerical flux functions are monotone. This experiment shows,

	Test Problem 1, $\lambda = 0$		Test Problem 1, $\lambda = 1$	
level	L^1-difference	EOC	L^1-difference	EOC
0	0.758314	—	0.0119577	—
1	0.437173	0.794	0.0050082	1.256
2	0.231999	0.914	0.0020877	1.262
3	0.119190	0.960	0.0008286	1.333
4	0.060372	0.981	0.0003137	1.401
5	0.030378	0.990	0.0001165	1.429
6	0.015237	0.995	0.0000439	1.409

Table 1: L^1-difference and EOCs between curved approximate solution $u^h(T)$ and flat approximate solution $\bar{u}^h(T)$ from Test Problem 1 for different values λ of numerical diffusion.

	Test Problem 2		Test Problem 3		Test Problem 4	
level	L^1-difference	EOC	L^1-difference	EOC	L^1-difference	EOC
0	0.112518	—	0.0370831	—	0.115867	—
1	0.039167	1.523	0.0133379	1.475	0.035202	1.719
2	0.011223	1.803	0.0040350	1.725	0.009566	1.880
3	0.002984	1.911	0.0011216	1.847	0.002475	1.950
4	0.000772	1.951	0.0002992	1.906	0.000630	1.975
5	0.000197	1.967	0.0000778	1.944	0.000159	1.985
6	0.000053	1.891	0.0000199	1.966	0.000040	1.989

Table 2: L^1-difference and EOCs between curved approximate solution $u^h(T)$ and flat approximate solution $\bar{u}^h(T)$ from Test Problems 2, 3 and 4.

that under the assumptions from our convergence analysis $\mathcal{O}(h)$ is indeed the optimal order of convergence.

However, if we modify the numerical diffusion by setting $\lambda = \pi$ in the numerical flux functions we achieve EOCs between 1 and 2 as can be seen in Table 1, as well.

Test Problem 2 (Advection across the poles). Let the flux function f be defined by $f(u, x) = uW(x)$ for $x \in \mathbb{S}^2$. Initial values are given by $u_0(x) = \mathbb{1}_{\{x_1 > 0.15\}}(x)$. In order to get monotone numerical flux functions we set $\lambda = \frac{1}{2}\|\partial_u f\|_\infty = \pi$. For this test case we obtain EOCs of almost 2, cf. Table 2.

Test Problem 3 (Burgers along the latitudes). We choose a flux function of Burgers-type $f = f(u, x) = 1/2u^2V(x)$ for $x \in \mathbb{S}^2$ and initial values $u_0(x) = \mathbb{1}_{\{x_1 > 0.15\}}(x)$. In order to get monotone numerical flux functions we set $\lambda = \frac{1}{2}\|\partial_u f\|_\infty = \pi$ and obtain EOCs of almost 2, cf. Table 2.

Test Problem 4 (Fully two-dimensional problem). In this test problem we consider a flux function f such that the corresponding initial value problem is not equivalent to a family of one-dimensional problems. Note that the flux functions from the previous test problems have been of one-dimensional nature. To this end we define $f(x, u) = uV(x) + 1/2u^2W(x)$ for $x \in \mathbb{S}^2$ with initial values $u_0(x) = \mathbb{1}_{\{x_1 > 0.15\}}(x)$ and observe EOCs of almost 2, cf. Table 2.

Test Problem 5 (2nd order scheme applied to Test Problem 1). The

	Test Problem 5		Test Problem 6	
level	L^1-difference	EOC	L^1-error	EOC
0	0.777427	—	0.00362492	—
1	0.444068	0.808	0.00243102	0.576
2	0.233521	0.927	0.00112593	1.115
3	0.119553	0.966	0.00034768	1.700
4	0.060461	0.983	0.00012006	1.534
5	0.030400	0.992	0.00003713	1.693
6	0.015242	0.996	0.00001116	1.734

Table 3: L^1-difference and EOCs between second order curved approximate solution (which equals the exact solution in this case) and a second order flat approximate solution from Test Problem 5 and L^1-error between the exact solution from Test Problem 6 and its approximation by the second order finite volume scheme.

motivation of this test problem is to show that in general even higher order schemes, which are based on the flat finite volume schemes, are not able to achieve higher order convergence rates for smooth data. To this end, we apply a second order finite volume scheme (which is validated in Test Problem 6) to Test Problem 1. This scheme is based on the flat finite volume scheme of first order (cf. Subsection 2.3) with $\lambda = 0$ enhanced with a linear reconstruction and a second order Runge-Kutta method for time evolution. In Table 3 we observe EOCs of almost 1. Indeed, the application of a second order finite volume scheme to Test Problem 1 gives exactly the same convergence rates as a first order scheme since the linear reconstruction on each cell does not affect the numerical flux functions as f is independent of u. We like to point out that we do not have to compute the curved approximate solution as it coincides with the (constant) exact solution.

Test Problem 6 (Validation of the 2nd order scheme). This test problem serves as validation of the second order finite volume scheme. We consider smooth initial values

$$u_0(x) := \frac{1}{10}\, \mathbb{1}_{\{r(x)<1\}}(x)\, \exp\left(\frac{-2\left(1+r^2(x)\right)}{\left(1-r^2(x)\right)^2}\right)$$

with $r(x) := \frac{|x_0 - x|}{0.74}$ and $x_0 := (1,0,0)^T$ and a flux function $f(x,u) := uV(x)$, which transports the initial values around the sphere. For the error between the flat second order finite volume scheme (see Test Problem 5) and the exact solution EOCs significantly higher than 1 are shown in Table 3.

Test Problem 7 (Deforming Torus). We consider a deforming torus as computational domain Γ and $T = 4$ as final time. Within the time interval $[0,2]$ the right half of the torus undergoes compression whereas the left half is stretched, while $\Gamma(t)$ remains constant for $t \in [2,4]$. We choose a Burgers-type flux function $f = f(u,x) = \frac{1}{2}u^2(x_2, -x_1, 0)^T$ and constant initial values $u_0 \equiv 1$. The time step size is chosen dynamically for each time step such that stability is guaranteed. In Figure 1 the numerical solution is shown at four different times. Note that in spite of the constant initial values, a shock wave is induced due to the change of geometry (compression and rarefaction) and the nonlinearity of the flux function.

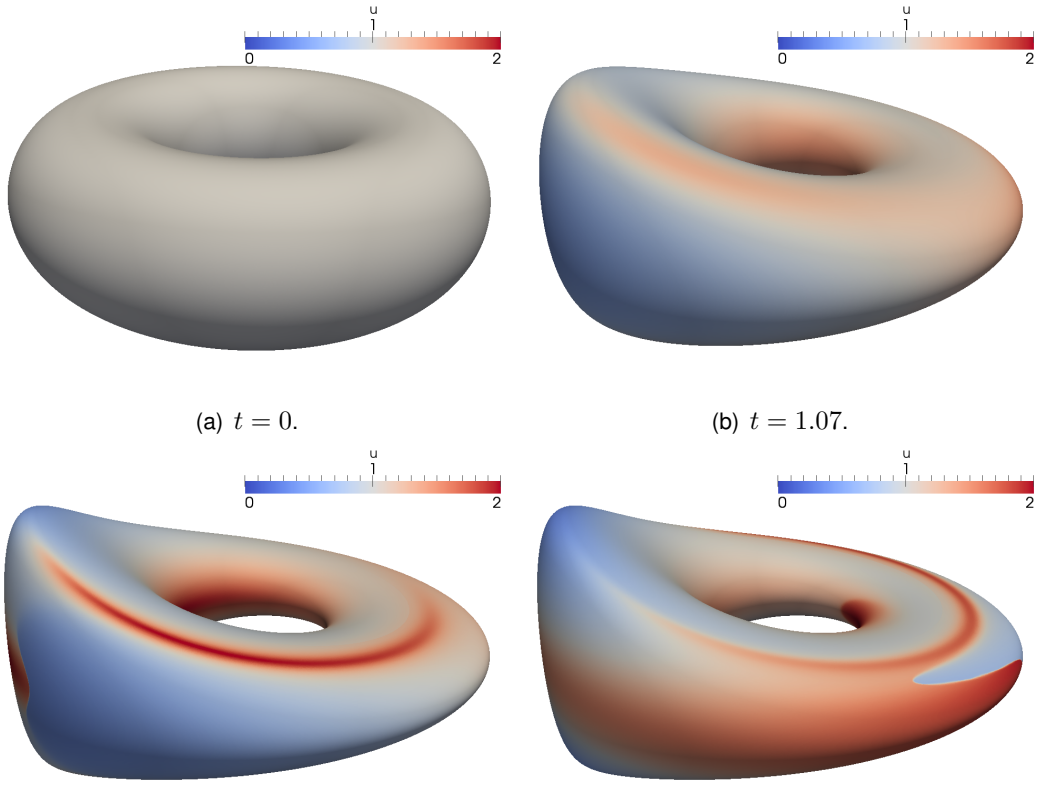

(a) $t = 0.$ (b) $t = 1.07.$

(c) $t = 2.36.$ (d) $t = 4.$

Figure 1: Flat approximate solution for Test Problem 7 for four different times. The computation was performed on a deforming polyhedron consisting of about 3 million. triangles.

5.2 Implementation Aspects

5.2.1 Software

All simulations have been performed within the DUNE-FEM module which is based on the Distributed and Unified Numerics Environment (DUNE) [8]. As coarsest grid approximating the sphere we use an unstructured grid consisting of 632 triangles, see Figure 2. For finer computations we refine the coarse macro grid (level 0) and obtain up to 2.5 million. triangles for the finest grid (level 6) whose vertices are projected onto the sphere, cf. Table 4.

level	h	size
0	0.033664	632
1	0.016833	2528
2	0.008416	10112
3	0.004208	40448
4	0.002104	161792
5	0.001052	647168
6	0.000526	2588672

Table 4: Different refinement levels of the sphere grid.

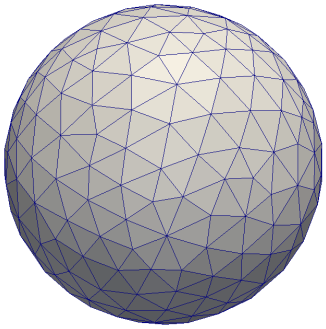

Figure 2: The sphere grid of level 0.

5.2.2 Exact Computation of Spherical Volume

For the curved finite volume scheme on the sphere the exact outer conormals, exact lengths of boundary segments and exact volumes of spherical triangles need to be computed. While the computation of the former two quantities is an easy geometric exercise, we use the formula from [26] for the computation of the latter.

5.2.3 Exact Computation of Numerical Flux Functions

For the exact evaluation of the numerical flux function corresponding to an edge e of a grid cell K, quantities of the form $\fint_e \langle V, \mu_{K,e}\rangle \, de$ have to be computed. Note that V can be written as $V = \nu \times \nabla h_V$ with $h_V(x) = 2\pi x_3$, where $\nu(x) := x$ denotes the outer unit normal to $\mathbb{S}^2$. As a result, similar to [10], we deduce

$$\fint_e \langle V, \mu_{K,e}\rangle \, de = \fint_e \langle \mu_{K,e} \times \nu, \nabla h_V\rangle \, de.$$

As $\mu_{K,e} \times \nu$ is a unit tangent vector to e, the integrand is a directional derivative along e and thus the integral can be computed by the evaluation at the endpoints of e. Obviously, the same applies to W with $h_W(x) = 2\pi x_2$ and $W = \nu \times \nabla h_W$.

5.2.4 Computation of L^1-Norms

We remark that the L^1-differences between the flat end the curved approximate solutions are computed on the triangulation Γ_h. This does not have any influence on the convergence rates.

Appendix

Here we give the proof of Lemma 4.4.

Proof. As we know that

$$\frac{|\bar{K}(t_n)|}{|\bar{K}(t_{n+1})|}, \frac{|K(t_n)|}{|K(t_{n+1})|}, \frac{|K(t_n)|}{|\bar{K}(t_{n+1})|} = 1 + \mathcal{O}(h), \ \frac{|K(t_n)|}{|\bar{K}(t_n)|} + \frac{|K(t_{n+1})|}{|\bar{K}(t_{n+1})|} = 2 + \mathcal{O}(h^2),$$

it is sufficient to prove

$$\left| \frac{|K(t_{n+1})|^2}{|K(t_n)|^2} - \frac{|\bar{K}(t_{n+1})|^2}{|\bar{K}(t_n)|^2} \right| \leq C|I_n|h, \tag{5.1}$$

to obtain both assertions of the Lemma.

Without loss of generality we assume the following situation: the triangle $K(t_n)$ is the convex hull of $(0,0,0), (h,0,0), (x,y,0)$. We define

$$\Phi^n(\cdot,t) : \Gamma(t_n) \to \Gamma(t), \quad \Phi^n(\cdot,t) := \Phi(\cdot,t) \circ \Phi(\cdot,t_n)^{-1},$$

such that $\Phi^n(\cdot,t_n)$ is the identity mapping. In addition we define for vectors $\mathbf{a}, \mathbf{b} \in \mathbb{R}^3$

$$\mathbf{a} \odot \mathbf{b} \in \mathbb{R}^{2\times 2}, \mathbf{a} \odot \mathbf{b} := \begin{pmatrix} \langle \mathbf{a}, \mathbf{a} \rangle & \langle \mathbf{a}, \mathbf{b} \rangle \\ \langle \mathbf{a}, \mathbf{b} \rangle & \langle \mathbf{b}, \mathbf{b} \rangle \end{pmatrix}.$$

and observe the identities

$$\|\mathbf{a} \times \mathbf{b}\|^2 = \det(\mathbf{a} \odot \mathbf{b}) \quad \text{and} \quad \det(\mathbf{a} \odot \mathbf{b}) = \det((\mathbf{a} + \lambda \mathbf{b}) \odot \mathbf{b}) \quad \forall \lambda \in \mathbb{R}. \tag{5.2}$$

We denote the canonical projection $\bar{K}(t_n) \to K(t_n)$ by c and abbreviate $\Phi^n \circ c$ by Φ^n_c. Obviously we have

$$|\bar{K}(t_n)| = \frac{1}{2}hy \tag{5.3}$$

and

$$\begin{aligned} 4|\bar{K}(t_{n+1})|^2 =& \| \left(\Phi^n((x,y,0),t_{n+1}) - \Phi^n((0,0,0),t_{n+1})\right) \\ & \times \left(\Phi^n((h,0,0),t_{n+1}) - \Phi^n((0,0,0),t_{n+1})\right) \|^2 \\ =& \det \Big(\left(\Phi^n(c(x,y,0),t_{n+1}) - \Phi^n(c(0,0,0),t_{n+1})\right) \\ & \odot \left(\Phi^n(c(h,0,0),t_{n+1}) - \Phi^n(c(0,0,0),t_{n+1})\right) \Big) \end{aligned}$$

as the vertices of $\bar{K}(t_n)$ and $K(t_n)$ coincide. Continuing the computation using (5.2) we get

$$
\begin{aligned}
&4|\bar{K}(t_{n+1})|^2 \\
&= \det\Bigg(\Big((x,y,0) + \int_{I_n} (\partial_\tau \Phi^n(c(x,y,0),\tau) - \partial_\tau \Phi^n(c(0,0,0),\tau))\, d\tau \Big) \\
&\quad \odot \Big((h,0,0) + \int_{I_n} (\partial_\tau \Phi^n(c(h,0,0),\tau) - \partial_\tau \Phi^n(c(0,0,0),\tau))\, d\tau \Big) \Bigg) \\
&= \det\Bigg(\Big((x,y,0) + \int_{I_n} \partial_y \partial_\tau \Phi^n_c((x_1,y_1,0),\tau) y + \partial_x \partial_\tau \Phi^n_c((x_2,y_2,0),\tau) x \, d\tau \Big) \\
&\quad \odot \Big((h,0,0) + \int_{I_n} (\partial_x \partial_\tau \Phi^n_c((x_3,0,0),\tau) h)\, d\tau \Big) \Bigg) \\
&= \det\Bigg(\Big((0,y,0) + \int_{I_n} \partial_y \partial_\tau \Phi^n_c((x_1,y_1,0),\tau) y d\tau \\
&\quad + \int_{I_n} (\partial_x \partial_\tau \Phi^n_c((x_2,y_2,0),\tau) - \partial_x \partial_\tau \Phi^n_c((x_3,0,0),\tau))\, x \, d\tau \Big) \\
&\quad \odot \Big((h,0,0) + \int_{I_n} (\partial_x \partial_\tau \Phi^n_c((x_3,0,0),\tau) h)\, d\tau \Big) \Bigg).
\end{aligned}
\tag{5.4}
$$

Combining (5.3) and (5.4) we get

$$
\begin{aligned}
&\frac{|\bar{K}(t_{n+1})|^2}{|\bar{K}(t_n)|^2} \\
&= \det\Bigg(\Big((0,1,0) + \int_{I_n} \partial_y \partial_\tau \Phi^n_c((x_1,y_1,0),\tau) d\tau \\
&\quad + \int_{I_n} (\partial_x \partial_\tau \Phi^n_c((x_2,y_2,0),\tau) - \partial_x \partial_\tau \Phi^n_c((x_3,0,0),\tau)) \frac{x}{y}\, d\tau \Big) \\
&\quad \odot \Big((1,0,0) + \int_{I_n} (\partial_x \partial_\tau \Phi^n_c((x_3,0,0),\tau))\, d\tau \Big) \Bigg) \\
&= 1 + \Big\langle (0,1,0), \int_{I_n} \partial_y \partial_\tau \Phi^n_c((x_1,y_1,0),\tau) d\tau \Big\rangle \\
&\quad + \Big\langle (0,1,0), \int_{I_n} (\partial_x \partial_\tau \Phi^n_c((x_2,y_2,0),\tau) - \partial_x \partial_\tau \Phi^n_c((x_3,0,0),\tau)) \frac{x}{y}\, d\tau \Big\rangle \\
&\quad + \Big\langle (1,0,0), \int_{I_n} (\partial_x \partial_\tau \Phi^n_c((x_3,0,0),\tau))\, d\tau \Big\rangle + \mathcal{O}(|I_n|^2).
\end{aligned}
\tag{5.5}
$$

Here we used that

$$
\det(A+B) = \det A + \mathrm{tr}_A(B) + \mathcal{O}(\|B\|^2),\ \forall A, B \in \mathbb{R}^{2\times 2}. \tag{5.6}
$$

Now we turn to the quotient of the areas of the curved faces and remark that

$$
|K(t_{n+1})| = |\Phi^n(K(t_n), t_{n+1})| + \mathcal{O}(|I_n|\, h\, |\bar{K}(t_{n+1})|), \tag{5.7}
$$

cf. [21] for a proof.

$$
\begin{aligned}
|\Phi^n(K(t_n), t_{n+1})| &= \int_{\bar{K}(t_n)} \sqrt{\det\left(\partial_x \Phi_c^n \odot \partial_y \Phi_c^n\right)} \\
&= \int_{\bar{K}(t_n)} \sqrt{\frac{\det\left(\partial_x \Phi_c^n \odot \partial_y \Phi_c^n\right)}{\det(\partial_x c \odot \partial_y c)}} \sqrt{\det(\partial_x c \odot \partial_y c)} \\
&= \sqrt{\frac{\det\left(\partial_x \Phi_c^n \odot \partial_y \Phi_c^n\right)}{\det(\partial_x c \odot \partial_y c)}}((x_4, y_4, 0), t_{n+1})|K(t_n)|.
\end{aligned} \tag{5.8}
$$

Using (3.6) we get for the quotient

$$
\begin{aligned}
&\frac{|K(t_{n+1})|^2}{|K(t_n)|^2} = \frac{\det\left(\partial_x \Phi_c^n \odot \partial_y \Phi_c^n\right)}{\det(\partial_x c \odot \partial_y c)}((x_4, y_4, 0), t_{n+1}) + \mathcal{O}(|I_n|h) \\
&= \frac{\left\| \left(\partial_x c + \int_{I_n} \partial_\tau \partial_x \Phi_c^n((x_4, y_4, 0), \tau) d\tau\right) \times \left(\partial_y c + \int_{I_n} \partial_\tau \partial_y \Phi_c^n((x_4, y_4, 0), \tau) d\tau\right) \right\|^2}{\det\left(\partial_x c \odot \partial_y c\right)} \\
&\overset{(5.6)}{=} 1 + \left\langle (1,0,0), \int_{I_n} \partial_\tau \partial_x \Phi_c^n((x_4, y_4, 0), \tau) d\tau \right\rangle \\
&\quad + \left\langle (0,1,0), \int_{I_n} \partial_\tau \partial_y \Phi_c^n((x_4, y_4, 0), \tau) d\tau \right\rangle + \mathcal{O}(|I_n|h).
\end{aligned} \tag{5.9}
$$

The statement of the Lemma follows by considering the difference of (5.9) and (5.5) and the fact that the smoothness of $\Phi^n \circ c$ only depends on the smoothness of Φ. □

References

[1] A. Alke and D. Bothe. 3d numerical modeling of soluble surfactant at fluidic interfaces based on the volume-of-fluid method. *Fluid Dynamics & Materials Processing*, 5(4):345–372, 2009.

[2] P. Amorim, M. Ben-Artzi, and P. G. LeFloch. Hyperbolic conservation laws on manifolds: total variation estimates and the finite volume method. *Methods Appl. Anal.*, 12(3):291–323, 2005.

[3] M. Ben-Artzi and P. G. LeFloch. Well-posedness theory for geometry-compatible hyperbolic conservation laws on manifolds. *Ann. Inst. H. Poincaré Anal. Non Linéaire*, 24(6):989–1008, 2007.

[4] M. R. Booty and M. Siegel. A hybrid numerical method for interfacial fluid flow with soluble surfactant. *J. Comput. Phys.*, 229:3864–3883, 2010.

[5] D. Bothe, J. Prüss, and G. Simonett. Well-posedness of a two-phase flow with soluble surfactant. In *Nonlinear elliptic and parabolic problems*, volume 64 of *Progr. Nonlinear Differential Equations Appl.*, pages 37–61. Birkhäuser, Basel, 2005.

[6] D. A. Calhoun, C. Helzel, and R. J. LeVeque. Logically rectangular grids and finite volume methods for PDEs in circular and spherical domains. *SIAM Rev.*, 50(4):723–752, 2008.

[7] B. Cockburn, F. Coquel, and P. G. LeFloch. An error estimate for finite volume methods for multidimensional conservation laws. *Math. Comp.*, 63(207):77–103, 1994.

[8] A. Dedner, R. Klöfkorn, M. Nolte, and M. Ohlberger. A generic interface for parallel and adaptive discretization schemes: abstraction principles and the DUNE-FEM module. *Computing*, 90(3-4):165–196, 2010.

[9] A. Demlow. Higher-order finite element methods and pointwise error estimates for elliptic problems on surfaces. *SIAM J. Numer. Anal.*, 47(2):805–827, 2009.

[10] D. Dziuk, D. Kröner, and T. Müller. Scalar conservation laws on moving hypersurfaces, SFB TR 71 Preprint, http://www.sfbtr71.de/publications/dziuk-kroener-mueller.pdf, submitted to Interf. Free Bound.

[11] G. Dziuk and C. M. Elliott. Finite elements on evolving surfaces. *IMA J. Numer. Anal.*, 27(2):262–292, 2007.

[12] G. Dziuk and C. M. Elliott. Surface finite elements for parabolic equations. *J. Comput. Math.*, 25(4):385–407, 2007.

[13] J. Giesselmann. A convergence result for finite volume schemes on Riemannian manifolds. *M2AN Math. Model. Numer. Anal.*, 43(5):929–955, 2009.

[14] J. Giesselmann and M. Wiebe. Finite volume schemes for balance laws on time-dependent surfaces. In *Numerical Methods for Hyperbolic Equations*, pages 251–258. CRC Press, London, 2012.

[15] P. A. Gilman. Magnetohydrodynamic ”shallow-water” equations for the solar tachocline. *The Astrophysical Journal Letters*, 544(1):L79–L82, 2000.

[16] F. X. Giraldo. High-order triangle-based discontinuous galerkin methods for hyperbolic equations on a rotating sphere. *J. Comput. Phys.*, 214(2):447–465, 2006.

[17] J. James and J. Lowengrub. A surfactant-conserving volume-of-fluid method for interfacial flows with insoluble surfactant. *J. Comput. Phys.*, 201(2):685 – 722, 2004.

[18] P. G. LeFloch and B. Okutmustur. Hyperbolic conservation laws on spacetimes. A finite volume scheme based on differential forms. *Far East J. Math. Sci. (FJMS)*, 31(1):49–83, 2008.

[19] P. G. LeFloch, B. Okutmustur, and W. Neves. Hyperbolic conservation laws on manifolds. An error estimate for finite volume schemes. *Acta Math. Sin. (Engl. Ser.)*, 25(7):1041–1066, 2009.

[20] D. Lengeler and T. MÃijller. Scalar conservation laws on constant and time-dependent riemannian manifolds. *J. Differential Equations*, 254(4):1705 – 1727, 2013.

[21] M. Lenz, S. F. Nemadjieu, and M. Rumpf. A convergent finite volume scheme for diffusion on evolving surfaces. *SIAM J. Numer. Anal.*, 49(1):15–37, 2011.

[22] E. Reister and U. Seifert. Lateral diffusion of a protein on a fluctuating membrane. *EPL*

(Europhysics Letters), 71(5):859, 2005.

[23] J. A. Rossmanith. A wave propagation algorithm for hyperbolic systems on the sphere. *J. Comput. Phys.*, 213(2):629–658, 2006.

[24] D. A. Schecter, J. F. Boyd, and P. A. Gilman. "shallow-water" magnetohydrodynamic waves in the solar tachocline. *The Astrophysical Journal Letters*, 551(2):L185–L188, 2001.

[25] H. A. Stone. A simple derivation of the time-dependent convective-diffusion equation for surfactant transport along a deforming interface. *Physics of Fluids A: Fluid Dynamics*, 2(1):111–112, 1990.

[26] A. Van Oosterom and J. Strackee. The solid angle of a plane triangle. *Biomedical Engineering, IEEE Transactions on*, BME-30(2):125 –126, 1983.

[27] D. L. Williamson, J. B. Drake, J. J. Hack, R. Jakob, and P. N. Swarztrauber. A standard test set for numerical approximations to the shallow water equations in spherical geometry. *J. Comput. Phys.*, 102(1):211–224, 1992.